PHOTONIC SENSORS / Vol. 14, No. 3, 2024: 240306

Development and Analysis of a Multi-Wavelength Near-Infrared Sensor for Monitoring Skin Hydration and Validation Using Monte Carlo Simulation

Iman GIDADO*, Raghda AL-HALAWANI,
Meha QASSEM, and Panicos KYRIACOU

Research Centre for Biomedical Engineering, City, University of London, London EC1V 0HB, UK

*Corresponding author: Iman GIDADO E-mail: iman.gidado@city.ac.uk

Abstract: The monitoring of an individual's hydration levels is a vital measurement required for the maintenance of a healthy skin barrier function as well as the avoidance of dehydration. The current commercial devices for this measure are typically based on electrical methodologies, such as capacitance, which allows for the extraction of skin hydration using the ionic balance deviations in the stratum corneum. The use of optical-based methods such as near-infrared spectroscopy (NIRS) has been recently explored for the measurement of skin hydration. Optical approaches have the ability to penetrate deeper into the skin layers and provide detailed information on the optical properties of present water bands. This paper presents the development of a multi-wavelength optical sensor and its capability of assessing skin hydration in an in vitro experiment utilizing porcine skin. Regression analysis of the results showed to be in line with standard reference measurements (R^2CV=0.952257), validating the accuracy of the developed sensor in measuring dermal water content. A Monte Carlo model of the human skin was also developed and simulated to predict the optical sensor's performance at variable water concentrations. This model serves as a tool for validating the sensor measurement accuracy. The output from this model gave a standard expectation of the device, which agreed with trends seen in the in vitro work. This research strongly suggests that non-invasive (wearable) NIR based sensors could be used for the comprehensive assessment of skin hydration.

Keywords: Skin hydration; NIRS; optical sensor; biosensors; wearables; Monte Carlo simulation

Citation: Iman GIDADO, Raghda AL-HALAWANI, Meha QASSEM, and Panicos KYRIACOU, "Development and Analysis of a Multi-Wavelength Near-Infrared Sensor for Monitoring Skin Hydration and Validation Using Monte Carlo Simulation," *Photonic Sensors*, 2024, 14(3): 240306.

1. Introduction

The hydration level of the skin is viewed as an important parameter to measure in specific applications. Key applications involve the use in cosmetics, hospital monitoring, and general wellbeing [1–3]. The stratum corneum is the layer of the skin with a direct interaction to obtain this measurement of hydration. This outermost layer controls the loss of water from the body via transepidermal water loss (TEWL), giving it the ability to regulate the dermal water content and thus control the barrier function of the skin, which provides protection from external influences and pathogens [4, 5].

Received: 28 August 2023 / Revised: 4 January 2024

DOI: 10.1007/s13320-024-0719-z
Article type: Regular

The current gold standard measurement device for skin hydration is the Corneometer® (Courage & Khazaka, Cologne, Germany), which uses the capacitance to obtain a reading based on the movement of ions and the current electrical properties of the skin [6]. Alternatively, optical techniques, such as near-infrared spectroscopy (NIRS), can be used to obtain information of deeper skin layers and give a better estimation of the water distribution due to these deeper depth profiles [7, 8]. However, current optical techniques involve the use of a benchtop spectrophotometer, which are typically expensive and large, making the need for a more portable (preferably wearable) optical device more favourable. Furthermore, wavelengths within the NIR region (750 nm to 2500 nm) include distinct water bands that are found in the skin, which can be easily distinguished and directly correlated to the skin water content [9, 10].

Optical NIRS sensors operate in the NIR range, penetrating the skin to assess hydration levels beyond the surface and providing insights into deeper tissue hydration. This capability makes NIRS valuable for non-invasive assessments, offering a more comprehensive understanding than surface sensors. However, challenges in measuring skin's water content with NIRS include the potential interference from ambient light, motion artifacts from subject movement, and variations in skin pigmentation affecting light absorption. Specific difficulties related to the penetration depth must be addressed, considering variations in the skin composition and structure among individuals. Calibration and standardization are crucial to ensure accurate interpretations of hydration levels at different tissue depths, enhancing the reliability and applicability of the findings [11].

Numerous in vitro studies have been previously carried out that involve the use of NIRS to measure skin hydration [12]. Qassem *et al*. [10, 13] conducted studies on both the porcine skin and human participants, exploring the properties of the stratum corneum in the NIR region. In vitro experiments revealed notably significant peaks visualizing typical water characteristics, which were seen at approximately 1 450 nm and 1 920 nm in the porcine skin spectra. This confirmed water presence in the porcine skin due to the higher light absorption at these water-specific wavelengths. In vivo experiments again showed expected peaks at 1 450 nm and 1 920 nm, but at a lower intensity. Beyond 1 900 nm, interference increased further, indicating deeper tissue saturation with water. Direct contact with the skin improved the identification of the water bands but presented occlusion risks, and thus overall non-contact readings were preferred. A single-fiber detector with a six-fiber source yielded the most reliable results.

A similar study by Kilpatrick-Liverman *et al*. [14] used an NIR optical fiber probe to assess skin water content variations with relative humidity (RH). In vitro experiments with porcine skin exposed to different RH levels demonstrated decreased water content as RH decreased, leading to a decline in absorbance of water peaks. In vivo experiments explored the effects of RH changes, humectants, and a choline spray on the skin water content, showing a direct correlation (R=0.83) between %RH and NIR readings.

The use of optical tissue probing with subsequent analysis is another optical technique for detecting human skin hydration. In an experiment which compared to the corneometer, an optical system developed by Kelman *et al*. [15] tracked back-reflected speckle patterns, presenting a significant decrease in the optical output over time after applying the moisturizer to the arm. Higher moisture levels correlated with faster fading of the acoustic wave, and the optical system showed a strong negative correlation (R=–0.87) with the corneometer. Unlike the corneometer, the optical system demonstrated a wide range of hydration readings and higher sensitivity to elevated hydration levels.

Additionally, a study conducted by Shen *et al*.

[16], comparable to the in vitro investigation carried out in this paper, investigated the utilization of an NIRS device (NIRONE S2.2 miniature NIR spectrometer) for characterizing the moisture content of both the porcine and human skin. Through a desorption experiment, the study revealed a robust linear relationship between the NIR spectra and the quantified moisture level, apparent through gravimetric decline via TEWL, with a linear regression correlation coefficient of 0.98. Furthermore, these findings were corroborated through an in vivo moisturizer study, where various moisturizers were applied to the arm, and their spectra were monitored over time, resulting in a 99.54% linear correlation with the skin moisture. In contrast to the present investigation, our study focused on the development of a more wearable device, diverging from conventional laboratory instruments and established spectrometers, as well as further exploring water-specific NIR wavelengths.

This paper describes the design and development of an optical sensor, consisting of multiple light-emitting diode (LED) wavelengths within the NIR range that are typical to attain absorption peaks related to water bands. The developed sensor was evaluated in vitro, utilizing the porcine skin and performing a weight-based desorption test. The reflectance signals from the sensor were compared and analysed against reference gravimetric and spectrophotometric measurements in order to extract the correlation coefficient to assess the accuracy of the developed sensor. A Monte Carlo (MC) simulation was also performed in order to confirm the sensor geometry and performance of the light-tissue interaction via the model imitating the designed optical sensor.

2. Materials and methods

2.1 Design and development of an optical hydration sensor

The photodiode used was the LAPD-09-17-LCC. It is an InGaAs (indium gallium arsenide) large area photodetector. InGaAs sensors have the high sensitivity and responsivity over wavelengths of 900 nm to 1700 nm. The LEDs used were dome lens infrared LEDs with wavelengths of 975 nm, 1050 nm, 1300 nm, and 1450 nm. The 1050 nm LED was used as the reference wavelength as there are no prominent water bands at 1050 nm. A casing was 3-dimensional (3D) printed to surround the printed circuit board (PCB) containing the optical components and consistently providing a 5 mm spacing between the sensor and a measurement sample, while avoiding effects from occlusion due to the direct contact. These are seen in Fig. 1, with the final sensor prototype, seen in Fig. 1(c).

The geometric parameters of the developed optical sensor were calculated to fit within a PCB at a distance as close as possible, thus the separation distance between the photodiode and each of the 4 LEDs was 5 mm. The total dimensions of the sensor and casing are annotated in Fig. 1 and seen next to a standard coin below, with the total weight being 9.9 g. The casing will incorporate an optical window and wrist straps to allow for a more wearable device during future in vivo studies.

In the sensor, two of the four LEDs were controlled at a time, with each LED managed by a constant current source to maintain the stable light emission. The emitted light interacted with skin components, and its absorption depended on the absorption coefficients at that specific wavelength to be converted to output voltages. The reflected and backscattered lights, influenced by skin optical properties, were detected by the photodiode proportional to the intensity of the detected light. The integration of LED control, a transimpedance amplifier, and conversion processes enhances the sensor's accuracy and reliability in assessing skin hydration levels.

The LEDs and photodiode anodes and cathodes were connected to a custom-made optical processing system (ZenPPG) [17]. The ZenPPG consisted of a transimpedance amplifier circuit to convert the

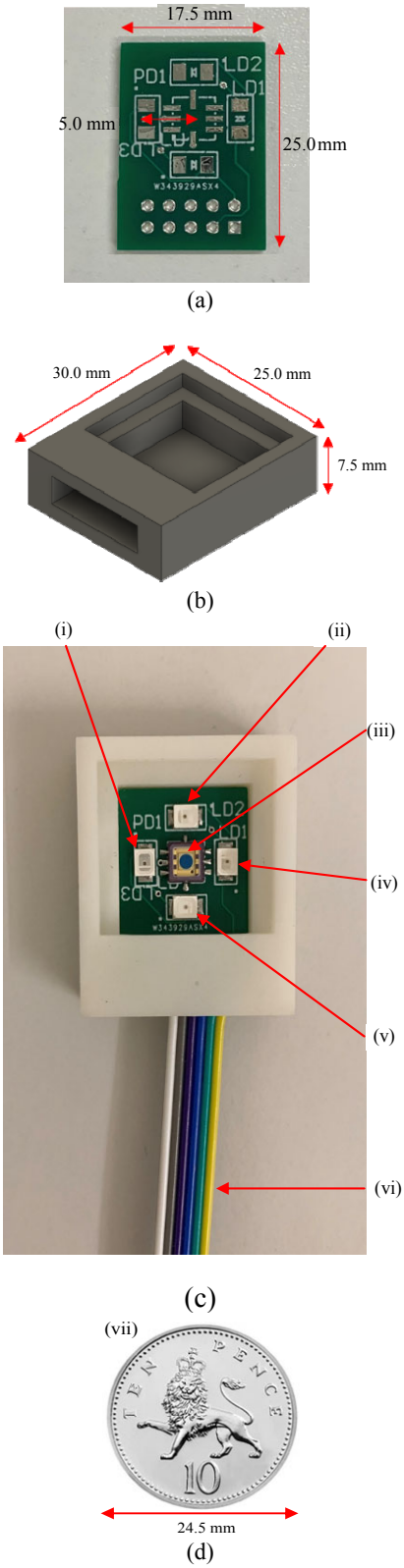

Fig. 1 Optical sensor prototype: (a) optical sensor PCB, (b) 3D printed device casing, and (c) optical sensor prototype [(i) 1300 nm LED, (ii) 1050 nm LED, (iii) InGaAs photodiode, (iv) 975 nm LED, (v) 1450 nm LED, (vi) wires connecting to ZenPPG and DAQ], and (d) coin comparison.

output current of the photodiode to a voltage, current sources to power the LEDs, a power board, and a core board containing a microcontroller. The output of the ZenPPG was connected to a computer via an NI data acquisition (DAQ) card (NI USB-6212, National Instruments, Austin, Texas, USA). These can be visualized below in Fig. 2. All optical signals, outputted as raw voltage values over time, were further pre-processed, displayed, and archived in a virtual instrument (VI) implemented in LabVIEW (2020 20.0.1, National Instruments, Austin, Texas, USA).

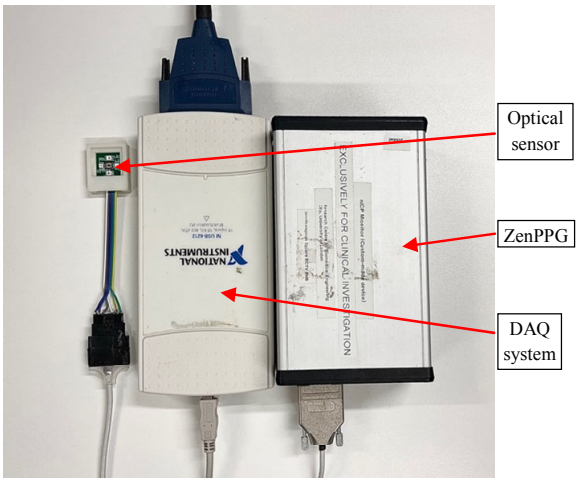

Fig. 2 Optical sensor prototype connected to the ZenPPG and DAQ system.

The results obtained from the optical sensor via LabVIEW were confirmed by comparison to both gravimetric measurements with a weight scale as well as spectral measurements with a spectrophotometer. The spectrophotometer used was an NIRQUEST+ (Ocean Insight, Florida, USA) near-infrared spectrometer. The reflectance readings from the spectrophotometer were facilitated using optical fibers and the output was sent to a computer with Oceanview software (Version 2.0, Ocean Insight, Orlando, Florida, USA). This software plotted the output spectra in real time for discrete readings to be saved as text files. Pre-processing of this data was completed on Spectragryph software (2022 v1.2.16, Freidrich Menges, University of Konstanz, Germany), which included the conversion of the reflectance measurements to apparent

absorbance spectra using the formula as

$$A = -\lg(1/R) \quad (1)$$

where A is the apparent absorbance and R is the reflectance, smoothing performed by a Savitzky-Golay filter and a baseline offset correction. For comparative reasons, the spectra obtained from the commercial spectrophotometer, along with the measurements obtained from the custom-made optical sensor were plotted and analysed in MATLAB (R2018b 9.5.0.944444, MathWorks, Massachusetts, USA).

2.2 In vitro experiment on the porcine skin

In vitro experiments were conducted on the porcine skin. This is due to the porcine skin being the most similar in terms of optical properties to the human skin and thus the most accurate to use for skin hydration studies. The experiment took place in a dark room to eliminate the effect of external light from the environment being detected by the optical sensors during the measurements. The protocol for the in vitro experiment first involved collecting fresh porcine skin from the local butcher. The porcine skin was then cut into a 50 mm×60 mm sample and was cleaned to remove any excess fat and connective tissue. The thickness of the porcine skin obtained ranged between 0.5 mm and 5.0 mm, with the sample being 3.0 mm thick.

The sample was placed in a petri-dish and into a humidity chamber set at 90% RH and 25℃ for 24 hr to ensure for the maximum hydration of the skin sample. The skin sample was then placed on an analytical balance (Scout STX, OHAUS, New Jersey, USA) with the developed optical sensor positioned on top of the right side of the sample and the reflectance optical fiber suspended over the left side of the sample. This setup allowed for simultaneous measurements of gravimetric readings as well as reflectance spectra and time series recordings. The total weight of the sample was then recorded with the analytical balance, with its initial wet weight being 33.15 g, and repeated every 20 min. Reflectance-voltage measurements from the developed optical sensor were continuously measured whereas the spectral data from the spectrophotometer were recorded every 20 min. The experiment continued with these measurements for a duration of 3 hr. The output data were extracted from Oceanview and LabVIEW for pre-processing on Spectragryph software and further comparison and analysis on MATLAB. The full in vitro setup is shown in Fig. 3.

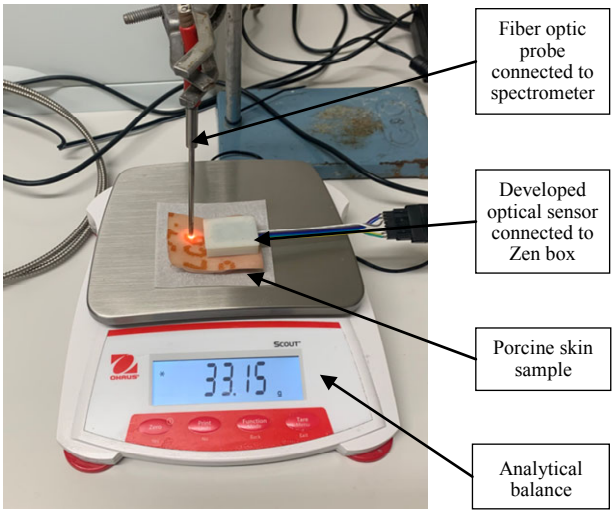

Fig. 3 Setup for the porcine skin in vitro experiment.

Pre-processing of the spectral data extracted from the spectrophotometer was performed using the Spectragryph software. This involved converting the reflectance measurements to apparent absorbance measurements, using (1). This essentially flipped the spectra across the x axis from 900 nm to 1 700 nm. The signals (spectra) were then cleaned using smoothing, specifically using Savitzky-Golay filtering with a set window of 21. The baseline offset was then corrected to allow for all the readings to be normalized by removing the initial baseline differences. For the developed optical sensor, a time series was extracted, measuring the changes in reflectance values over the duration of the experiment, being 120 s duration. The data were extracted and imported directly into MATLAB for comparisons and further analysis.

2.3 MC simulation to model optical interactions of the skin

An MC model is a mathematical computational tool used to predict the outcome of systems that rely on random processes. By using this technique, a model of the human skin was developed and simulated, and subsequently attempted to replicate the photon pathway using the optical measurement device. The predicted outcomes from this model were compared to the results obtained from the in vitro experiment on the porcine skin using the developed optical device. Human skin properties were used in this model since optical properties for the porcine skin is known to be similar to that of humans.

The model utilized the pseudo random generator, which was assigned to the variable(s) in question, to replicate the stochastic nature of photons in the human tissue. The human finger is made up of skin, fat, muscle, and bone in reverse order. The skin is made up of six layers, namely the stratum corneum, epidermis, papillary dermis, upper blood net dermis, reticular dermis, and deep blood net dermis. The following MC model was adapted to imitate the light-tissue interactions seen in the porcine skin as the water concentration changes. Firstly, it considered only the behaviour of photons in the skin and fat layers, since the porcine sample used in the in vitro setup was made out of these two layers. Secondly, the model did not account for perfused skin and hence neglected the effects of blood and level of oxygenation. As a result, the absorption coefficients of all the skin layers were equal and denoted by $\sqrt{\mu_{a\text{skin}}}$. A semi-infinite 3D model, with coordinates (x, y, z) and direction cosines $\left(\sqrt{u_x}, \sqrt{u_y u_z}\right)$, was developed to represent the spherical nature of photons. The total thickness (magnitude of the z-axis) of the region under investigation was 1.45 mm; the optical properties, which were obtained from the literature, were used to simulate and predict the light-tissue interactions at the source detector separation of 5 mm; the water concentration was varied between 0% and 100%. The simulation was run for 10^7 photons, with each photon assigned a "weight", i.e., intensity, equal to unity before it entered the tissue. Reflectance was quantified by calculating the sum of detected photon intensity, given by the weight of the photons which decreased over time due to surface reflection and fractional absorption at each interaction site.

As previously noted, the model involved the inclusion of variable inputs for the optical properties of the region of interest at the set wavelengths. These selected values can be seen in Table 1 [18–21] for the scattering coefficients (μ_s) measured in mm^{-1}, conveying the ability of the light photons to be absorbed and scattered per unit distance, respectively. The anisotropy factor (g) was also included to account for the directionality of the photons when they were scattered. The absorption coefficients (μ_a) of skin were calculated from the MC model for each wavelength at the different water concentrations.

Table 1 Optical properties of skin layers at selected wavelengths used in the MC model from the literature.

Wavelength(nm)	975			1 300			1 450		
Properties	μ_a	μ_s	g	μ_a	μ_s	g	μ_a	μ_s	g
Skin	–	17.5	0.904	–	15.15	0.903	–	11.3	0.873
Fat	1.06	8	0.862 5	0.89	8.5	0.927 5	1.05	10.5	0.93
Water	0.051 4	0	0	0.134	0	0	3.17	0	0

3. Results

3.1 Reference gravimetric measurement comparison for spectrophotometer spectra

Figure 4 shows the gravimetric readings of the porcine skin that were obtained every 20 min across the 3-hr experimental time period. A direct negative linear relationship can be seen, conveying a decrease in the weight of the sample over time. This expected trend was due to the evaporation of water from the skin sample via transepidermal water loss (TEWL). Weight is commonly used experimentally as a reference for investigating novel methodologies due to a direct quantitative output, as seen in Fig. 4.

The raw reflectance spectra as displayed on the Oceanview software interface were extracted as data points for each 20-min reading. The graphs plotted on MATLAB are illustrated in Fig. 5(a).

The raw R spectra were also converted to absorption spectra via the application of the Lambert-Beer law, as seen in Fig. 5(b). As mentioned in Section 2.2, further pre-processing of the spectral data was performed that involved smoothing of the signal using Savitzky-Golay filtering followed by the removal of baseline differences via normalisation techniques.

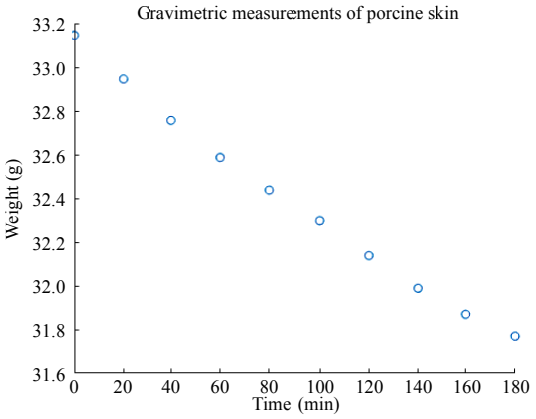

Fig. 4 Recorded gravimetric measurements during the desorption test of the experiment.

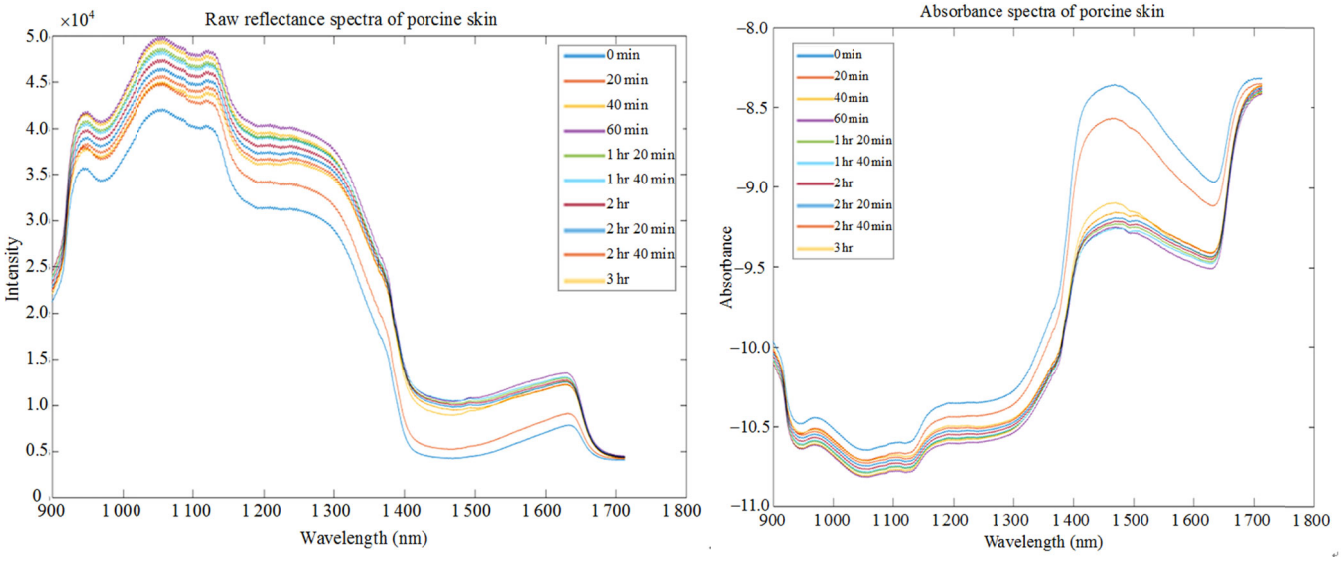

(a) (b)

Fig. 5 Spectrophotometric output of desorption test: (a) raw reflectance spectra of the porcine skin sample at 20-min time intervals and (b) converted absorbance spectra of the porcine skin sample at 20-min time intervals.

The reflectance spectra obtained from the spectrophotometer in this in vitro experiment were converted to absorbance spectra in order to analyse the peaks present. The absorbance spectra shown in Fig. 5(b) show the most distinct peaks at 975 nm and 1450 nm. These peaks are due to the water bands that are apparent at these wavelengths. Chemical analysis of the peaks suggests that at these particular

wavelengths, there is a sufficient amount of energy provided by the LED that allows for the excitation of certain chemical bonds, for example, the OH bonds present in water. This high energy level breaks these bonds and produces the output that is seen as an increased peak in the absorption spectra.

On the other hand, the reflectance spectra have an inverse relationship with the absorption spectra, presenting the amount of light that has not been absorbed by the sample being measured but reflected back to the detector. These reflectance values in particular will be used further for comparisons to the developed optical sensor as it utilizes the same optical methodology, yet as a time series of discrete wavelengths that are known to be sensitive to producing water bands in spectra.

3.2 Assessing spectral agreement between developed optical sensor and spectrophotometer

The output from the developed optical sensor provided reflectance data points as voltages over time for each of the 4 independent wavelengths. Therefore, 4 time series across the 3-hr period were extracted and plotted on MATLAB. As 1050 nm is the wavelength with the least distinct water peaks present, it was used as the baseline reference wavelength. The signal produced by the 1050 nm LED was subtracted from the signals of the other 3 wavelengths. This avoids for the application of further post-processing techniques by correcting shifts from external effects and allows for better graphical visualisation. These optical outputs can be seen in Fig. 6.

The output reflectance spectra obtained from the spectrophotometer were converted to time series plotted by extracting the discrete reflectance voltage values at the different time points for each of the 3 wavelengths (975 nm, 1300 nm, and 1450 nm), giving 10 extracted time point outputs. This spectrophotometer reflectance time series was used as a reference to compare to the reflectance time series of the developed optical sensor. It was conveyed from the data that there was a similar trend presenting an increase in reflectance values over time due to evaporation of water from the sample. This supports the suggestions that as water content decreases, absorption decreases and thus reflectance increases. Moreover, this confirms that the developed sensor works similarly to the spectrophotometer. All recorded output reflectance data for both the developed sensor and the spectrophotometer were used to plot the given reflectance output values. When looking at these measurements of the porcine skin sample over time in Fig. 4, its linear relationship can be portrayed to complement the trend of both reference techniques. Both the developed sensor and the spectrophotometer display a positive trend of reflectance with respect to an increase in time, suggesting a decrease in absorbance due to less water bands present within the sample. This relatively displays as an increase in reflectance due to the inverse relationship between these spectral measures. Furthermore, when solely comparing the spectral time series of the 2 sensors, a positive correlation can be visualized, which confirms the similarities of the readings obtained from the developed sensor to that of a gold standard spectrophotometer and increases its validity as a measure. This has also been plotted at its 9 timepoints as a line graph in Fig. 7, which likewise presents similarities between the techniques in the coordinative trend of larger deviations in reflectance at high water contents before an expected plateau over time, with significantly increased sensitivity to changes at 1450 nm.

Figure 7 re-plots the developed sensor output displayed in Fig. 6 alongside the spectrophotometer output at its set intervals in order to provide a more optimal reference comparison.

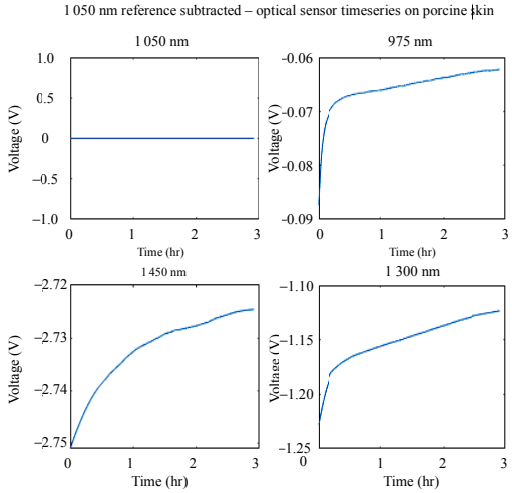

Fig. 6 Time series of the developed optical sensor on the porcine skin for the 4 LED wavelengths over time after the subtraction of the 1 050 nm reference wavelength.

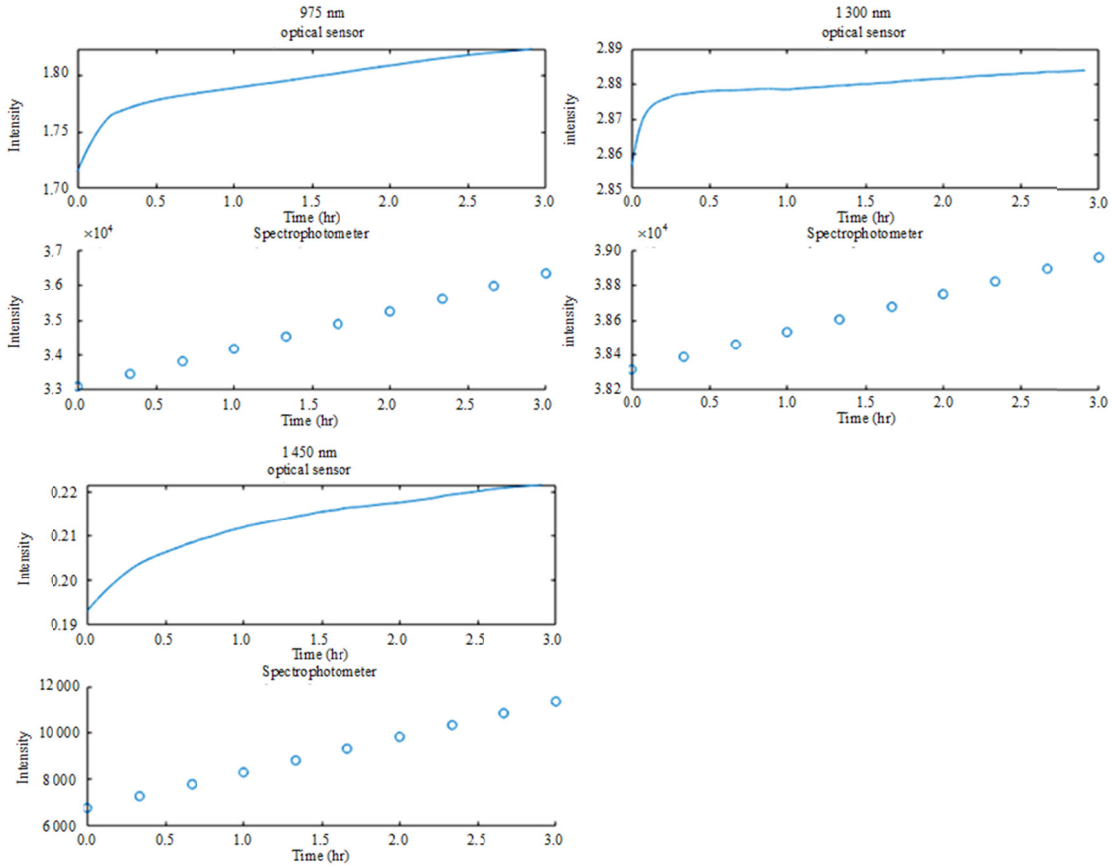

Fig. 7 Reflectance time series of the optical sensor on the porcine skin for the 4 wavelengths over time after subtraction of 1 050 nm LED output (line) compared to the spectrophotometer output (circles).

The developed sensor and spectrophotometer output both convey a positive correlation between reflectance and time, thus with a decrease in the water weight. Therefore, this implies a decrease in absorbance due to fewer water bands present in the skin. Figure 8 displays the optical sensor LEDs and spectrophotometer reflectance output, presenting the expected positive trend with water loss over time,

which is more apparent at higher water concentrations of the sample followed by a steady plateau. These trends also correspond positively with the gravimetric weight measurements, further confimring that the increase is due to the loss in water weight over time. Moreover, in terms of the comparison of the developed sensor to the standard spectrophotometer, a positive trend is visualised between the two, further enhancing the validity of measurements with the optical sensor. This will further be analysed for assessing the measurement accuracy using regression techniques, which is demonstrated later in this paper.

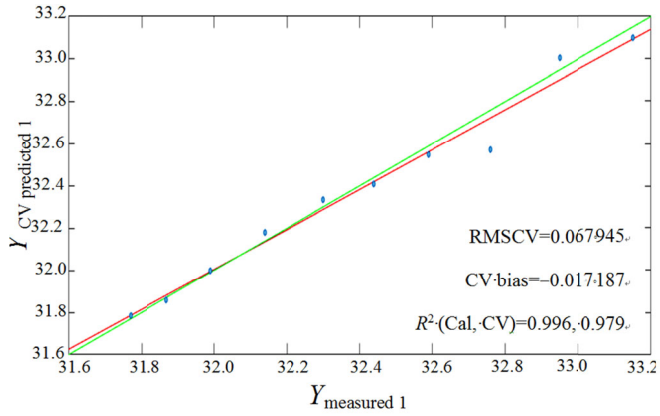

(a)

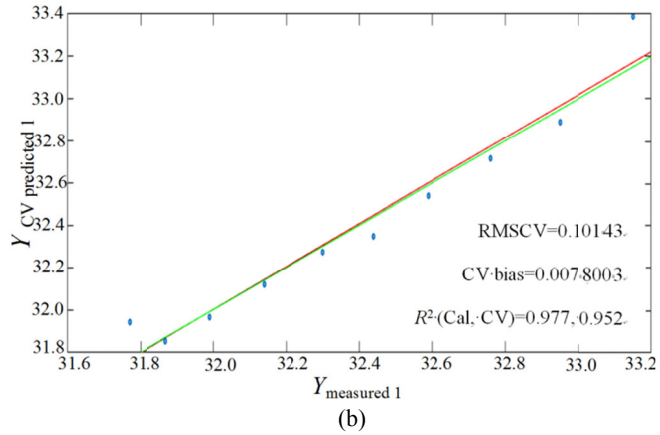

(b)

Fig. 8 Output scores extracted from regression techniques: (a) partial least squares (PLS) regression output of the spectrophotometer (red) and gravimetric (green) measurements and (b) multiple linear regression (MLR) output correlation plot of the developed optical sensor (red) and gravimetric (green) measurements.

3.3 Analysis of agreement using regression techniques

In order to evaluate the correlations between the measured results and the reference, regression techniques are required. For comparisons of the independent wavelengths chosen within the developed optical sensor to the gravimetric readings, the calculation of the Pearson correlation coefficient is established. This correlation coefficient, R, measures the linear relationship between 2 variables and the strength of this association. The p-value is used to convey the statistical significance of the correlation if the obtained R values conclude a difference from 0 in population. In this experiment, it was expected that there would be a negative correlation present, since a decrease in the weight and water content of the porcine skin sample related to an increase in the measured reflectance readings. Table 2 displays the calculated R and p-values at these individual LED wavelengths. It can be seen in the table that 975 nm has a weaker correlation, which could also be seen by the highest p-value out of the 3 wavelengths. However, all R values have presented the expected strong negative correlation to the gravimetric reference. This means that there is a high tendency for X variable scores, being the device measurements, to go with low Y variable scores, being the gravimetric readings (and vice versa). Furthermore, these significantly strong correlation coefficients seen for the developed sensor, signifies the high measurement accuracy and reliability. Moreover, the strong negative correlations alongside extremely low p-values is more prominent at the wavelengths of 1 300 nm and 1 450 nm, signifying the presence of more distinct water bands at these wavelengths and the increased sensitivity of the bands with the developed sensor, which has been proved [12].

Table 2 Pearson correlation coefficients of sensor's independent wavelengths vs gravimetric measurements.

	R	p-value
975 nm LED vs gravimetric measurements	−0.8486	0.001936
1300 nm LED vs gravimetric measurements	−0.9899	<0.00001
1450 nm LED vs gravimetric measurements	−0.9285	0.000105

The PLS regression was also used to model and analyse the covariance between the entire spectral output of the spectrophotometer and the reference

gravimetric measurements. The PLS has the ability to quantify the relationship between 2 sets of data by constructing linear predictive models. The PLS regression is useful in this case due to the predictors being collinear and the spectral measurements containing a large number of variables. Unlike principal components regression (PCR), the PLS takes into account variance and measures the predictors with errors, increasing the robustness and measurement accuracy of the model [22]. Eigenvector's PLS_Toolbox (R9.2, Eigenvector Research, Washington, USA) was installed on MATLAB, where the data were inputted into the PLS model, involving cross validation via Venetian blinds with 5 splits, in order to assess the predictive capability of the model. The output data extracted from this model were the calibration coefficient of determination (R^2 Cal.), cross-validation coefficient of determination (R^2 CV), bias, CV bias, root mean standard error for calibration (RMSEC), and root mean standard error for cross-validation (RMSECV), as well as the graphical scores.

On the other hand, the MLR was the regression technique used for analysing the relationship of the developed optical sensor with the reference gravimetric measurements. The MLR correlates 2 datasets by calculating the distance to a fully linear relationship, being $y = \mathrm{m}x + \mathrm{b}$ [23]. This regression model was used as the data obtained from the developed data were single intensity points denoting the reflectance value at a specific point in time, as oppose to a spectral output requiring PLS. Three sets of these reflectance data recordings were obtained, as there were 3 LED wavelengths acting as the model's independent variables. The same outputs were extracted for the MLR as the PLS which allowed for comparative analysis purposes.

The results displayed in Table 3 conveyed a noticeably high R^2 for the cross-validation of 0.952257 with the developed optical sensor, which was an extremely strong correlation coefficient to the reference variables. In comparison, the spectrophotometer had an R^2 value of 0.978974, with a difference of 0.026717 to the developed sensor being minimal, enhancing its ability to perform similarly to a gold standard device. Also, it could be seen that the likelihood of affecting errors was low in both cases for the RMSECV, but relatively lower for the developed sensor in the cross validation alongside a significantly lower bias than the spectrophotometer. This enhanced the measurement accuracy of this developed sensor and its ability to outperform a standard spectrophotometer. The differences in bias and RMSECV could be explained by the fact that the developed sensor consisted of independent wavelengths that were most sensitive to water bands within the skin and therefore did not have as much influence from other constituents of the skin. Although the regression values were very close between the 2 devices, it was expected the spectrophotometer would conduct higher scores, even though the difference was seen to be very small. However, the developed sensor with 3 sole wavelengths had been shown to be able to sufficiently detect variations in the water content almost equally to that of a full range measurement device, questioning the need for the additional wavelengths not directly related to water bands.

In addition, the results displayed in Fig. 8 present the scores extracted from the regression models. The figures show the plots for the measured and predicted outcomes against a directly correlated line. It can be seen in Fig. 8(b), being the MLR scores for the developed sensor, the plotted points are extremely close to the expected line, signifying the strong predictive accuracy, which can also be similarly portrayed from the scores from the spectrophotometer output in Fig. 8(a).

These scores allow for the correlation between the x and y score variables to be established as well as the strength of the linear agreement. This positive linear correlation consisting of very few outliers

from the predicted correlation line indicates that as one variable changes, the mean of the other variable has almost the exact trend, which can be suggested in engineering that the variables can be considered from the same system.

Table 3 MLR and PLS regression outputs of the developed sensor and spectrophotometer to gravimetric measurements.

Output parameters	R^2 Cal.	R^2 CV	Bias	CV bias	RMSEC	RMSECV
Reference spectrophotometer PLS	0.996 331	0.978 974	0.000 103 921	−0.017 871	0.026 788 4	0.067 944 8
Developed optical sensor MLR	0.977 32	0.952 257	0.000 036 902 1	0.007 800 34	0.066 654 3	0.101 431

3.4 MC characterization

The MC model generated reflectance outputs for all water concentration conditions at three wavelengths (975 nm, 1300 nm, and 1450 nm). Figure 9 shows the average reflectance across 0% and 100% water concentrations in increments of 10% at the three selected wavelengths. As expected, the reflectance is seen to increase as the water concentration decreases for all wavelengths, imitating the loss of water due to evaporation from the skin. This is illustrated in Fig. 9, which plots the average reflectance against decreasing water concentration intervals, showing a positive trend. At the wavelength of 1450 nm, it is known that there is an extremely distinct water band present, thus explaining the increased steepness in its plots at higher water concentrations in comparison to other wavelengths. Consequently, the average reflectance is also plotted using a logarithmic scale for the better visualisation of the data.

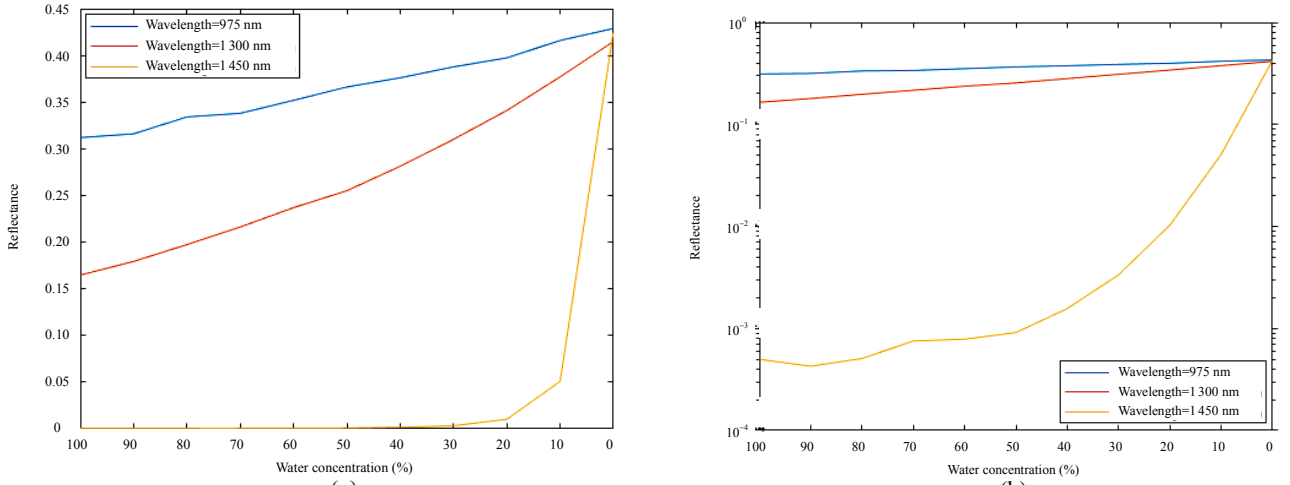

Fig. 9 Average reflectance output as the water concentration changes at 975 nm, 1300 nm, and 1450 nm: (a) linear scale and (b) logarithmic scale.

In addition, photon profiles were generated after simulating the current MC model, illustrating the movement of detected photons as they travelled between the source and the photodetector via backscattering. These were plotted for 0% and 100% water concentrations for each of the three wavelengths, seen in Figs. 10 and 11, for the purposes of illustrating and comparing the extremes of water concentration. Visually, it can be seen that there are differentiations between the 0% and 100% water concentrations, with the higher water content displaying an increase in the number of detected photons. Clear differences in the number of scattering events (indicated by the brighter regions) can also be visualized among the three different wavelengths, signifying that the wavelengths with higher intensity water bands, such as 1450 nm, will absorb a higher number of photons. This leads to a decrease in the number of photons reaching the photodetector and the intensity displayed in the

profile maps of the detected photons.

Due to the significantly higher absorption coefficient of water at the 1450 nm (3.17 mm^{-1}, Table 4), there is an extremely small number of detected photons at the 100% water concentration (Fig. 11).

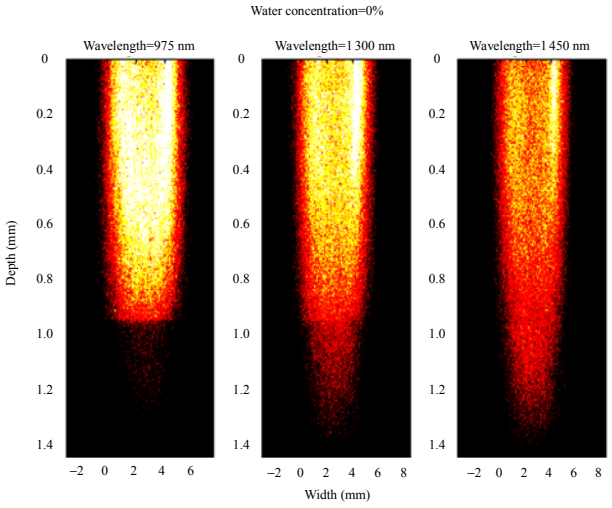

Fig. 10 Simulated photon profiles for the skin at a water concentration of 0% at 3 selected wavelengths.

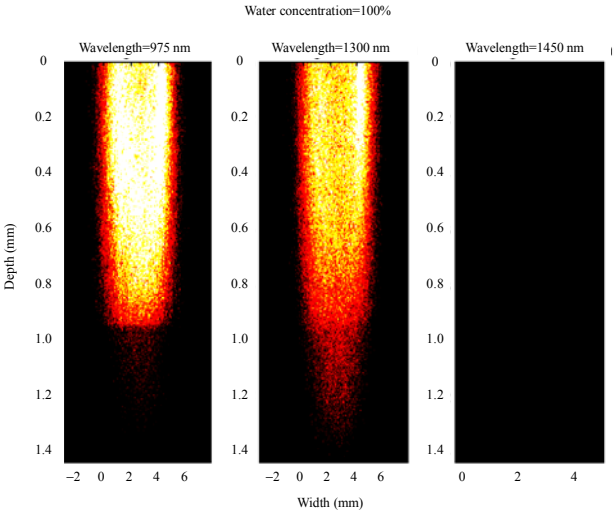

Fig. 11 Simulated photon profiles for the skin at a water concentration of 100% at 3 selected wavelengths.

Table 4 Calculated stratum corneum (SC) absorption coefficients (mm^{-1}) of water concentrations at 975 nm, 1300 nm, and 1450 nm in 10% intervals.

Water coefficient (%)	Wavelength (nm)		
–	975	1 300	1 450
0	0.014 6	0.005 7	0.004 0
10	0.018 3	0.018 6	0.320 6
20	0.022 0	0.031 4	0.637 2
30	0.025 7	0.044 2	0.953 8
40	0.029 3	0.057 0	1.270 4
50	0.033 0	0.069 9	1.587 0
60	0.036 7	0.082 7	1.903 6
70	0.040 4	0.095 5	2.220 2
80	0.044 0	0.108 3	2.536 8
90	0.047 7	0.121 2	2.853 4
100	0.051 4	0.134 0	3.170 0

4. Discussion and conclusions

The need for skin hydration measurement devices based on optical techniques has been found to be significantly advantageous to the gold standard electrical methodologies [14, 15, 24]. The acquisition of optical properties within the skin can give more accurate correlations to the water content present due to the distinct water bands. These are more clearly seen when using wavelengths within the NIR region, which also allows for an increased penetration depth. A wearable or portable skin hydration measurement device can be used to improve the monitoring of the wellbeing of individuals, whether it is in general health and athletics or for those suffering from skin diseases and requiring the testing of moisturizers to aid in this.

This paper describes in detail the design and development of a near-infrared optical sensor for measuring skin hydration via reflectance of the skin surface. The LED wavelengths were chosen to be

975 nm, 1300 nm, and 1450 nm, with a reference wavelength of 1050 nm.

An in vitro experiment was conducted on the porcine skin using a custom-made optical sensor, which is most similar to the human skin and can be hydrated to different levels using an environmental chamber. The results of this experiment involved a reference of gravimetric measurements indicating the loss of the skin water content over time due to evaporation, via a desorption test, to then compare with the measured spectra. With a decrease in weight measurements of the skin sample, there was seen to be an increase in the reflectance measurement from both sensors. This confirmed that as the porcine skin was becoming more dehydrated, the absorbance was also declining, and thus there was an increase in the reflectance readings due to its inverse relationship to absorption. Moreover, in terms of comparison of the developed sensor to the standard spectrophotometer, a positive trend was visualized between the two, further enhancing the validity of measurements with the optical sensor. The pattern seen in the plot of the percentage water loss for each of the techniques was also presented to be of complimentary trends. This trend of water loss displayed a larger percentage of water evaporating from the skin sample at the start of the experiment followed by a plateau as the water content became more minimal. In addition, both techniques were seen to detect greater fluctuations from the 1450 nm LED than the others, agreeing with the intensity of the water absorption bands present at this wavelength, leading to a significantly increased sensitivity [8–9].

Regression techniques, involving multiple linear regression and partial least squares, were used to assess the strength of the correlations between the 2 optical devices, the developed sensor and a standard spectrophotometer, to the reference gravimetric measurement. The outputs of these methods showed high R^2 values for the cross validation in both cases, with the spectrophotometer only having a very slight increase. However, the bias and error calculation for the developed sensor was significantly lower than those of the spectrophotometer, signifying the increased measurement accuracy on top of the high correlation coefficients obtained. These results were able to enforce the ability of the developed optical device to effectively measure changes in the dermal water content with the high accuracy.

In order to validate the suitability of the developed sensor design, an MC simulation was also used, in which the exact distances between the sources and detectors as well as the selected wavelengths were inputted. The model was successful in providing the expected reflectance outputs in all cases, as well as photon profiles displaying the pathway of the detected photons. It was seen that within the skin layer, being less than 1 mm in thickness, a significantly higher number of scattering events were occurring relative to the fat layer. This was displayed across all wavelengths, although 1450 nm showed a lower overall penetration depth of detected photons. Due to the high absorption coefficients of the distinct water peak present at this wavelength, fewer incident photons reached the photodetector, since many photons were absorbed before reaching the photodetector.

Additionally, an increased number of detected photons was apparent at the 0% water concentration in comparison to 100%, more so at the 1450 nm wavelength due to the significant water absorption peak present. This suggests that the presence of water in the skin leads to the greater absorption at these wavelengths and a decreased intensity of the detected signal, complementing the trend seen in the experimental results. The results obtained from the output of the MC simulation were able to confirm the reliability and validity of the sensor's specifications and its ability to measure skin hydration.

The study's use of the porcine skin prompts questions about the applicability of the optical sensor

and NIR water absorbance model for applying direct moisture detection on the human skin. The spectra of the human skin generally conform to the shape of porcine skin spectra, which predominantly reflect the O-H absorption signal in water. Despite shared similarities, the dynamic nature of the human skin can present challenges for optical detection, unlike the static porcine skin. In addition, the penetration depth of NIR photons can also be disadvantageous, as it can potentially reach the blood layer, which can be a constituent that affects the accuracy of skin moisture assessment, as well as this not being present within the porcine skin sample. It should be noted that these complexities are vital for translating findings and applying the developed technology to reliably detect moisture on the human skin. Furthermore, to handle this dynamic nature of the human skin, incorporating motion correction algorithms and continuous monitoring in the sensor design may be required. The optimization of wavelength selection and exploration of multi-spectral analysis help minimize interference from blood, addressing penetration depth issues. Developing a human skin-specific calibration through extensive in vivo studies ensures the sensor's adaptability to individual variations. The integration of real-time feedback mechanisms and machine learning algorithms can enable the sensor to dynamically adjust to differing skin conditions. This will aim to make the optical sensor accurate, adaptable, and ethically reliable for human skin measurements [25, 26].

TEWL is influenced by the water vapor pressure gradient between the skin surface and its surrounding environment. The higher moisture content in the air can potentially reduce this pressure gradient, leading to a decrease in TEWL measurements. Therefore, controlling and standardizing the environmental conditions, particularly air moisture, is crucial for achieving accurate and reproducible TEWL measurements in in vitro experiments [27].

There can also be an impact on the measurement accuracy due to pore shrinkage on light reflection in the skin during such experiments. Pore shrinkage can alter the skin's optical properties and affect the scattering and absorption of incident light. Pores in the skin can act as scattering centres for light, and changes in these pore sizes may lead to variations in the reflection and absorption of light. This can influence the results of the optical measurements related to skin hydration and other properties [28]. Validation methods are essential to interpret the optical results accurately, especially with structural changes, such as pore shrinkage. Advanced imaging methods, such as confocal microscopy or optical coherence tomography, can provide more detailed information about the skin structure and help assess the impact of these changes on light interaction [29].

There are many other factors to consider but all cannot be accounted for, e.g., skin texture and colour. We have selected wavelengths that are known to be most specific to water, being our main analyte, therefore we will be able to obtain a high enough signal-to-noise ratio to obtain a signal related mainly to the water content. Exploratory studies typically prioritize obtaining valid results within defined parameters, which is the case in this paper. While such studies provide meaningful information, subsequent experiments with improved control measures may be necessary to confirm and refine these initial observations, establishing more robust results to extract direct relationships.

Future work within this area involves the further aesthetic development of the optical sensor, to allow it to be more user friendly and explore the possibility of a wearable device. Calibration techniques will also be utilized to ultimately find a relationship among the 3 output values at different wavelengths and combine them into a single output reading or value. Also, future in vivo experiments are currently being conducted to assess the ability of the developed optical sensing device on humans and their ability to detect small changes in the skin water content. These in vivo experiments are currently

being carried out to test the developed optical device on different populations, for example, to assess the effect of different skin tones on skin hydration and in the exploration of the effect of hydrators and moisturizers on different skin types. The exploration of the device's ability to accurately measure an individual's body hydration and its relationship with skin hydration values will also be focused on within these future studies. This will allow for further validation of the device's measurement accuracy, confirming its ability to perform sufficiently under different applications and conditions.

Declarations

Conflict of Interest The authors declare that they have no competing interests.

References

[1] N. Pross, "Effects of dehydration on brain functioning: a life-span perspective," *Annals of Nutrition and Metabolism*, 2017, 70(Suppl. 1): 30–36.

[2] T. Montero-Vilchez, M. V. Segura-Fernández-Nogueras, I. Pérez-Rodríguez, M. Soler-Gongora, A. Martinez-Lopez, A. Fernández-González, *et al*., "Skin barrier function in psoriasis and atopic dermatitis: transepidermal water loss and temperature as useful tools to assess disease severity," *Journal of Clinical Medicine*, 2021, 10(2): 359.

[3] R. J. Maughan and S. M. Shirreffs, "Dehydration and rehydration in competative sport," *Scandinavian Journal of Medicine & Science in Sports*, 2010, 20(s3): 40–47.

[4] F. H. Martini and J. L. Nath, "*Fundamentals of Anatomy & Physiology*," 8th edition. San Francisco: Pearson, 2008.

[5] E. Jéquier and F. Constant, "Water as an essential nutrient: the physiological basis of hydration," *European Journal of Clinical Nutrition*, 2010, 64(2): 115–123.

[6] Princeton Consumer Research, "*Skin moisturizer clinical trials | moisturization testing*," online available: https://www.princetonconsumer.com/moisturization-testing/.

[7] R. M. Balabin, R. Z. Safieva, and E. I. Lomakina, "Comparison of linear and nonlinear calibration models based on near infrared (NIR) spectroscopy data for gasoline properties prediction," *Chemometrics and Intelligent Laboratory Systems*, 2007, 88(2): 183–188.

[8] LSBU, "Water_absorption_spectrum.pdf," online available: https://www.idc-online.com/technical_references/pdfs/chemical_engineering/Water_absorption_spectrum.pdf.

[9] A. M. C. Davies, "An introduction to near infrared (NIR) spectroscopy | IM Publications Open," Retrieved March 8, 2024 from https://www.impopen.com/introduction-near-infrared-nir-spectroscopy.

[10] M. Qassem and P. A. Kyriacou, "In vitro spectrophotometric near infrared measurements of skin absorption and dehydration," in *2012 Annual International Conference of the IEEE Engineering in Medicine and Biology Society*, San Diego, USA, 2012, pp. 6044–6047.

[11] S. L. Zhang, C. L. Meyers, K. Subramanyan, and T. M. Hancewicz, "Near infrared imaging for measuring and visualizing skin hydration. A comparison with visual assessment and electrical methods," *Journal of Biomedical Optics*, 2005, 10(3): 031107.

[12] I. M. Gidado, M. Qassem, I. F. Triantis, and P. A. Kyriacou, "Review of advances in the measurement of skin hydration based on sensing of optical and electrical tissue properties," *Sensors*, 2022, 22(19): 7151.

[13] M. Qassem. and P. A. Kyriacou, "*In vivo optical investigation of short term skin water contact and moisturizer application using NIR spectroscopy*," in Annual International Conference of the IEEE Engineering in Medicine and Biology Society, Osaka, Japan, 2013, pp. 2392–2395.

[14] L. Kilpatrick-Liverman, P. Kazmi, E. Wolff, and T. G. Polefka, "The use of near-infrared spectroscopy in skin care applications," *Skin Research and Technology*, 2006, 12(3): 162–169.

[15] Y. T. Kelman, S. Asraf, N. Ozana, N. Shabairou, and Z. Zalevsky, "Optical tissue probing: human skin hydration detection by speckle patterns analysis," *Biomedical Optics Express*, 2019, 10(9): 4874.

[16] X. Shen, S. Lan, Y. Zhao, Y. Xiong, W. Yang, and Y. Du, "Characterization of skin moisture and evaluation of cosmetic moisturizing properties using miniature near-infrared spectrometer," *Infrared Physics & Technology*, 2023, 132: 104759.

[17] K. Budidha, V. Rybynok, and P. A. Kyriacou, "Design and development of a modular, multichannel photoplethysmography system," *IEEE Transactions on Instrumentation and Measurement*, 2018, 67(8): 1954–1965.

[18] A. N. Bashkatov, E. A. Genina, and V. V. Tuchin, "Optical properties of skin, subcutaneous, and muscle tissues: a review," *Journal of Innovative Optical Health Sciences*, 2011, 4(1): 9–38.

[19] E. Zamora-Rojas, B. Aernouts, A. Garrido-Varo, D. Pérez-Marín, J. E. Guerrero-Ginel, and W. Saeys, "Double integrating sphere measurements for estimating optical properties of pig subcutaneous adipose tissue," *Innovative Food Science & Emerging Technologies*, 2013, 19: 218–226.

[20] A. N. Bashkatov, "Optical properties of the subcutaneous adipose tissue in the spectral range 400 to 2500nm," *Optics and Spectroscopy*, 2005, 99(5): 836–842.

[21] C. W. Robertson and D. Williams, "Lambert absorption coefficients of water in the infrared," *Journal of the Optical Society of America*, 1971, 61(10): 1316–1320.

[22] S. Wold, M. Sjöström, and L. Eriksson, "PLS-regression: a basic tool of chemometrics," *Chemometrics and Intelligent Laboratory Systems*, 2001, 58(2): 109–130.

[23] A. Hayes, "Multiple linear regression (MLR) definition, formula, and example," online available: https://www. investopedia.com/terms/m/mlr.asp.

[24] H. Arimoto and M. Egawa, "Non-contact skin moisture measurement based on near-infrared spectroscopy," *Applied Spectroscopy*, 2004, 58(12): 1439–1446.

[25] A. K. L. Fujita, R. W. da Rocha, A. Escobar, A. B. de Nardi, V. S. Bagnato, and P. F. C. de Menezes, "Correlation between porcine and human skin models by optical methods," *Human Skin Cancers – Pathways, Mechanisms, Targets and Treatments*, London: IntechOpen, 2018.

[26] M. Mamouei, S. Chatterjee, M. Razban, M. Qassem, and P. A. Kyriacou, "Design and analysis of a continuous and non-invasive multi-wavelength optical sensor for measurement of dermal water content," *Sensors*, 2021, 21(6): 2162.

[27] M. Green, N. Kashetsky, A. Feschuk, and H. I. Maibach, "Transepidermal water loss (TEWL): environment and pollution – a systematic review," *Skin Health and Disease*, 2022, 2(2): e104.

[28] A. M. Ionescu, J. Chato-Astrain, J. D. L. C. Cardona, F. Campos, M. M. Pérez, M. Alaminos, *et al*., "Evaluation of the optical and biomechanical properties of bioengineered human skin generated with fibrin-agarose biomaterials," *Journal of Biomedical Optics*, 2020, 25(5): 1.

[29] C. Ruini, B. Kendziora, E. Z. Ergun, E. Sattler, C. Gust, L. E. French, *et al*., "In vivo examination of healthy human skin after short-time treatment with moisturizers using confocal Raman spectroscopy and optical coherence tomography: preliminary observations," *Skin Research and Technology*, 2022, 28(1): 119–132.